Available online at www.sciencedirect.com
SCIENCE DIRECT
Physica D 215 (2006) 25–37
PHYSICA D
www.elsevier.com/locate/physd

From trigger to phase waves and back again

Grigori Bordiougov*, Harald Engel

Institut für Theoretische Physik, Technische Universität Berlin, Hardenbergstrasse 36, 10623 Berlin, Germany

Received 7 October 2004; received in revised form 23 June 2005; accepted 4 January 2006
Available online 14 February 2006
Communicated by Y. Kuramoto

Abstract

Transitions between trigger and phase waves are studied using a reaction–diffusion model, which admits both types of travelling wave activity. It is demonstrated that the transition from trigger waves to phase waves is preceded by qualitative changes in the dispersion relation of the former. These changes in dispersion in turn are provided by modified decay properties behind a solitary pulse. At high values of excitability the dispersion curve of trigger waves is destroyed upon a transcritical collision with the dispersion curve of phase waves, so both types of waves turn out to be connected in the small-wavelength region. As an important part of the study we present the results on the linear stability analysis of the waves close to the transition threshold. In particular, the stability of trigger waves with wiggly dispersion is thoroughly scrutinized and the stability of phase waves close to the transcritical collision is analyzed as well. We accompany our studies with one-dimensional simulations of the transition between phase and trigger waves under variation of the control parameter.

Keywords: Trigger waves; Phase waves; Excitation pulses; Stability; Active media; Shilnikov homoclinics

1. Introduction and motivation

Both trigger and phase waves belong to the basic types of the patterns in active media and can arise in many physical, chemical and biological systems [1,2]. Typical examples of such nonlinear dissipative waves include the well-known Belousov–Zhabotinsky (BZ) reaction [3], excitations of heart muscle, pulse propagation in nerves, calcium waves in living cells, etc. [4].

Trigger waves are typical for excitable media [5], where an element of such a medium can produce a burst of activity, triggered by a supra-threshold perturbation, produced by the diffusional flow from its neighborhood. After the activity burst, the element of the excitable medium slowly relaxes to the typically stable rest state. The velocity of such waves depends strongly on the diffusion. Trigger waves can propagate either alone or form trigger wave trains. Spatially periodic trigger wave trains can be characterized by a dispersion curve, which describes the dependence of the wave train velocity c on its wavelength L. In the following we will use the term "trigger waves" for both solitary and spatially periodic structures.

Phase waves are merely phase-shifted oscillations of the bulk of the medium; they exist if the kinetics of the underlying reaction–diffusion system is oscillatory. The propagation velocity of phase waves is reciprocal to the initially introduced phase gradient, resulting in a linear dispersion curve. The diffusion does not significantly affect their velocity. The dynamics of phase waves can be well understood in generic models like amplitude equations [6,4]. In the parameter plane including the wavenumber k and the time scale ratio ϵ there are well-known regions of existence and stability of such waves. The stability boundaries are the Eckhaus boundary [7] and the so-called zigzag boundary [8]. Phase waves in real systems like the BZ reaction are often considered to be produced by an inhomogeneity, which introduces a phase gradient in stable homogeneous bulk oscillations [9].

One of the first theoretical studies on the transition between trigger and phase waves in a model of the Zhabotinsky reaction was presented in [10]. In the case of oscillatory kinetics trigger waves can coexist with phase waves. If the velocity of the phase wave is smaller than the velocity of the coexisting trigger wave, the former can initiate a new trigger wave. A stricter distinction

* Corresponding author. Tel.: +49 175 247 8282.
E-mail address: greg@physik.tu-berlin.de (G. Bordiougov).

0167-2789/$ - see front matter © 2006 Elsevier B.V. All rights reserved.
doi:10.1016/j.physd.2006.01.005

between phase and trigger wave trains, based on the analysis of the shape of the dispersion curves was proposed in [11]. First, it was demonstrated that up to a certain wavelength phase and trigger waves have roughly the same dispersion (inflection point I in Fig. 1). Then, depending on the type of the wave, under further increase of the wavelength the velocity of the wave can either grow infinitely — this corresponds to the phase waves — or saturate, approaching the limit c_0. In the latter case the wave is of trigger type and c_0 is the velocity of the solitary excitation pulse.

At the same time many qualitatively different types of dispersion curves for trigger waves were found [12], which can be classified into: (i) monotonic where $c(L)$ is a monotonously increasing function that asymptotically approaches a maximum value which equals the velocity of the solitary pulse c_0, (ii) non-monotonic with a negative slope domain, corresponding to attraction between neighboring pulses, and (iii) oscillatory with damped oscillations giving rise to alternating attractive and repulsive pulse interaction. The first case is called normal dispersion, while the last two possibilities are referred to as anomalous dispersion.

The more interesting case, namely oscillatory dispersion, is shown to be provided by the oscillatory decay of excitation behind a solitary pulse. It often occurs close to a supercritical Andronov–Hopf bifurcation in the kinetics of the reaction–diffusion system. Due to the oscillation in the pulse tail, one can construct infinitely many equally spaced wave trains with wavelengths ranging up to infinity moving with the same velocity [13,14]. The resulting wave train changes its stability depending on the interpulse distance periodically [14,15]. Experimental evidence for oscillatory dispersion was reported as well, for example, in gas discharge experiments [16]. Moreover, the interaction between the oscillatory tail and the head of the successive pulses can be so strong that it leads to locking-type phenomena, described theoretically in [17–19]. Such locking results in the coexistence of two stable pulse trains with the same wavelength, but different propagation velocities.

There are many examples that in the same reaction–diffusion system both kinds of waves can exist at different parameter values [3], but the question of the transition between those wave types remains to our knowledge open. Moreover, waves at the boundary between phase and trigger dynamics are rich in instabilities, which can lead to new patterns like trace- and backfiring [20]. The purpose of the present paper is to *capture the bifurcation scenario of the transition* between two types of waves in specific details, including the stability of waves in the transition region. The analysis of travelling waves is reduced to the study of their profiles and velocities in the so-called travelling wave ODE (profile ODE) under the assumption that the propagation velocity of the waves is constant.

First, we describe the origin of trigger and phase waves. Spatially periodic trigger wave trains are constructed of infinitely many periodic replications of the primary solitary pulse. In the phase space of the travelling wave ODE the limit cycles, representing these wave trains, exist close to the homoclinic solution, describing the primary solitary pulse.

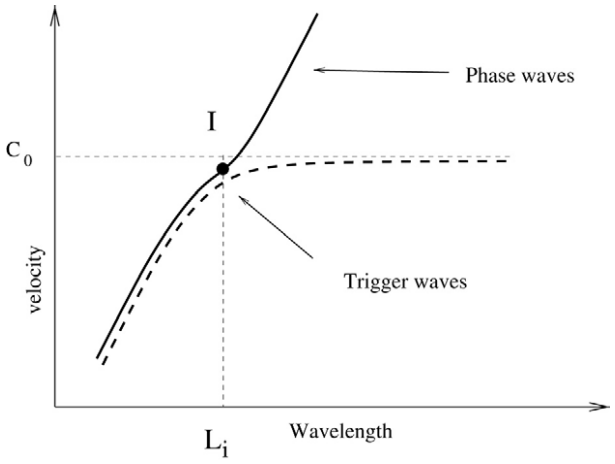

Fig. 1. Dispersion curves of phase waves (solid thick line) and dispersion of trigger waves (dashed thick line). They nearly coincide up to some wavelength L_i. The velocity of trigger waves has limit c_0 — the velocity of a solitary pulse. I denotes the inflection point.

The profile of phase waves is represented by periodic solutions that stem from an Andronov–Hopf bifurcation of the homogeneous rest state of the PDE. In the limit of large wavelengths, trigger wave trains converge to the solitary pulse with finite velocity. The profile of phase waves of large wavelengths approximates the shape of the limit cycle in the kinetics of the reaction–diffusion system under infinite increase of the propagation velocity. However, the large-wavelength limit is not always accessible in experiments (for example, spiral waves usually send out short-wavelength wave trains), that is why we are interested in the connection between trigger and phase waves in the short-wavelength region.

Upon varying the control parameter from the regime of trigger waves to the regime of phase waves, we first observe twisted trigger wave dispersion, which is essentially provided by the oscillatory decay behind the solitary pulse. After the Andronov–Hopf bifurcation in the appropriate co-moving frame, a branch of phase waves appears. At the critical point the dispersion curve of phase waves collides with the dispersion curve of trigger waves in the region of small wavelengths. The curve of the dispersion of the trigger waves collapses in a series of saddle-node bifurcations. The only dispersion curve, which persists in the "wavelength–velocity" parameter plane, is the dispersion of phase waves.

In order to get a thorough insight in the studied transition, we discuss in detail the stability properties of both types of waves close to the transition threshold. The stability of trigger waves with wiggly dispersion are exhaustively described. A good agreement between the slope of the dispersion curve and the curvature of the spectrum in the origin is found numerically. We elaborate the stability of the phase waves close to the transition region as well and show that phase waves first appear as unstable small-amplitude patterns and then stabilize, reaching large amplitude. We support our studies of the conversion between trigger and phase waves by one-dimensional simulations, which can be thought of as the first starting point for experimental proof of our results.

2. Model, methods and main results

2.1. Model

In this paper, as a representative model displaying for appropriately chosen parameter values both oscillatory as well as excitable kinetics, we consider the two-component Oregonator model modified to describe the photosensitive variant of the BZ reaction [21]. In this reaction trigger and phase waves have been extensively studied for a long time [2]. The equations for the dimensionless concentration of bromous acid, u, and the oxidized form of the catalyst, v, read

$$\partial_t \mathbf{u} = \mathbf{f}(\mathbf{u}) + \mathbf{D}\partial_x^2 \mathbf{u}, \tag{1}$$

where

$$\mathbf{u} = \begin{pmatrix} u \\ v \end{pmatrix},$$

$$\mathbf{f} = \begin{pmatrix} F(u,v) \\ G(u,v) \end{pmatrix} \equiv \begin{pmatrix} \frac{1}{\epsilon}\left[u - u^2 - (fv+\phi)\frac{u-q}{u+q}\right] \\ u - v \end{pmatrix} \tag{2}$$

and $\mathbf{D} = \mathrm{diag}\,(D, 0)$.

Diffusion of v is omitted because in most experiments the catalyst is immobilized in a gel matrix. The time scale ratio ϵ follows from the recipe concentrations [21]. In this paper, all parameters except ϕ are fixed at the following values $\epsilon = 0.05$, $f = 2.1$ and $q = 0.002$. The parameter ϕ is proportional to the intensity of applied illumination. It will be considered as the main bifurcation parameter which controls the local dynamics as well as the profile and the velocity of different wave solutions, playing the role of the "excitability" parameter in the system.

The Oregonator kinetics

$$\begin{aligned} \dot{u} &= \frac{1}{\epsilon}\left[u - u^2 - (fv+\phi)\frac{u-q}{u+q}\right], \\ \dot{v} &= u - v \end{aligned} \tag{3}$$

belongs to the wide class of activator–inhibitor models with two well-separated time scales (ϵ is assumed to be small) and a typical "s"-shaped nullcline $F(u, v) = 0$ (see Fig. 2(b) and (c) for a sketch of nullclines $F(u, v) = 0$ and $G(u, v) = 0$). With the chosen parameters the Oregonator kinetics (3) has only one fixpoint, which undergoes a supercritical Andronov–Hopf bifurcation at ϕ_{hb} (see Fig. 2). It is convenient to use ϕ_{hb} as a reference point for other bifurcations, say, for the stability threshold of solitary pulses. Under further decrease of ϕ the stable limit cycle born at ϕ_{hb} passes through a so-called canard explosion at ϕ_c and its size rapidly grows up. Detailed analysis of such bursting behavior and its relation to the excitability properties of the spatially extended system was presented in [22].

It is important to note that for $\phi_c < \phi < \phi_{hb}$ the system is still excitable, supporting high-amplitude excitation pulses, which relax to the small limit cycle around the unstable fixpoint.

2.2. Coherent structure approach

We study stationary solutions of the full PDE (1) which move with constant velocity c. Transforming to a co-moving frame $\xi = x - ct$, Eq. (1) becomes

$$\partial_t \mathbf{u} = \mathbf{f}(\mathbf{u}) + c\partial_\xi \mathbf{u} + \mathbf{D}\partial_\xi^2 \mathbf{u}. \tag{4}$$

A stationary solution propagating with velocity c corresponds to the condition $\partial_t \mathbf{u} = 0$. In this case we can reduce the problem to the so-called travelling wave ODE for the spatial profile of the solution:

$$\mathbf{f}(\mathbf{u}) + c\partial_\xi \mathbf{u} + \mathbf{D}\partial_\xi^2 \mathbf{u} = 0, \tag{5}$$

or in the following form:

$$\begin{aligned} \dot{\mathbf{u}} &= \mathbf{v}, \\ \mathbf{D}\dot{\mathbf{v}} &= -\left[c\mathbf{v} + \mathbf{f}(\mathbf{u})\right], \quad \dot{*} \equiv \partial_\xi *. \end{aligned} \tag{6}$$

In our case $\mathbf{D}$ is singular and the profile equations read:

$$\begin{aligned} u_\xi &= w, \\ v_\xi &= -\frac{1}{c}(u - v), \\ w_\xi &= -\left[cw + \frac{1}{\epsilon}\left(u - u^2 - (fv+\phi)\frac{u-q}{u+q}\right)\right]. \end{aligned} \tag{7}$$

We see immediately that if $\mathbf{u}_0$ is a fixpoint of the kinetics then $(\mathbf{u}_0, \mathbf{0})$ is also a fixpoint in the system (6).

Within this approach, a solitary excitation pulse which runs on a spatially homogeneous background $\mathbf{u}_0$ corresponds to a homoclinic orbit to equilibrium $(\mathbf{u}_0, \mathbf{0})$ in (5) (Fig. 3(b)). A periodic wave train in the RD-system (1) is presented by a limit cycle in the travelling wave ODE (Fig. 3(a)). Both types of solutions can be successfully tracked with the continuation software AUTO [23] along the parameters of the nonlinearity $\mathbf{f}(\mathbf{u})$, the velocity c and the wavelength L.

2.3. Stability of waves

For a comprehensive understanding of the transition between phase and trigger waves a detailed stability analysis of the underlying wave solutions turned out to be essential. Moreover, as only stable travelling wave solutions can be observed experimentally, stability considerations are crucial for future experimental verification of our results.

To study the stability of the solutions to the RD-equation we use a straight-forward approach, linearizing the equation about the studied solution [24]. The eigenvalues of the obtained linear operator are the growth rates of small perturbations: instability of the solution is reflected by the existence of eigenvalues with positive real parts.

For a given solution $\mathbf{u}_0(\xi)$ of (4) we can formulate the corresponding eigenvalue problem:

$$\mathcal{M}\mathbf{w} \equiv \mathbf{f}_\mathbf{u}(\mathbf{u}_0(\xi))\mathbf{w} + c\partial_\xi \mathbf{w} + \mathbf{D}\partial_\xi^2 \mathbf{w} = \lambda \mathbf{w}, \tag{8}$$

where $\mathbf{w}$ is an eigenfunction of $\mathcal{M}$, and $\mathbf{f}_\mathbf{u}$ denotes the linearization of the function $\mathbf{f}$.

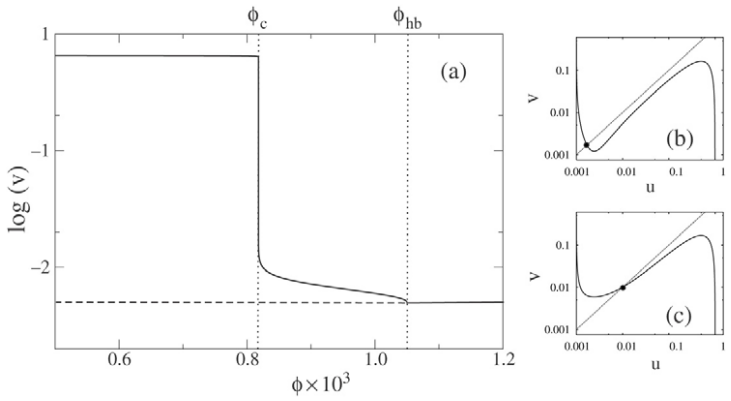

Fig. 2. (a) Bifurcation diagram of the kinetics described by Eq. (1). With the chosen parameter values for ϵ, f and q (compare text) an Andronov–Hopf bifurcation occurs at $\phi_{hb} = 1.04 \times 10^{-3}$. For the canard point we find $\phi_c = 0.81 \times 10^{-3}$. The full line shows the amplitude of oscillations around the unstable fixpoint (dashed line) below ϕ_{hb}. (b) Nullclines of the kinetics (2) above the Andronov–Hopf bifurcation. The full (dashed) line denotes the u- (v-) nullcline, respectively. (c) The same as (b) but below the ϕ_{hb}-point.

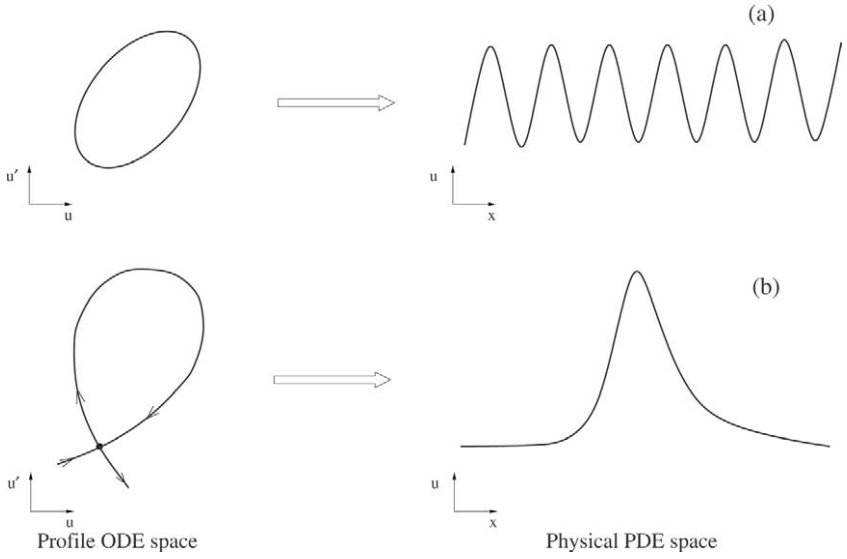

Fig. 3. Representation of different travelling patterns in travelling wave ODE phase space. (a) A limit cycle represents a wave train. (b) A homoclinic connection represents a solitary pulse.

We distinguish between two parts of the eigenvalue spectrum of the operator $\mathcal{M}$ (see [24,25] and references therein for strict mathematical definitions). The first one is called the essential spectrum and depends on the asymptotic behavior of the operator $\mathcal{M}$ as $\xi \to \pm\infty$. The corresponding eigenfunction occupies the whole space. The second part of the spectrum is called the point spectrum and consists of isolated eigenvalues. The eigenfunctions belonging to isolated eigenvalues are localized and decay exponentially to zero as $\xi \to \pm\infty$. The point spectrum describes the stability of the localized structures of the solution, for example, the stability of a solitary pulse, which propagates on a homogeneous background. In the case of periodic wave trains and homogeneous rest states the point spectrum is empty.

For a L-periodic solution $\mathbf{u}_0(\xi) = \mathbf{u}_0(\xi + L)\lambda$ is an eigenvalue of $\mathcal{M}$ if the following system

$$\begin{aligned} &\mathbf{f}_{\mathbf{u}}(\mathbf{u}_0(\xi))\mathbf{w} + c\partial_\xi \mathbf{w} + \mathbf{D}\partial_\xi^2 \mathbf{w} = \lambda \mathbf{w}, \quad 0 < \xi < L, \\ &(\mathbf{w}, \partial_\xi \mathbf{w})(L) = e^{2\pi(\eta + i\gamma)}(\mathbf{w}, \partial_\xi \mathbf{w})(0) \end{aligned} \tag{9}$$

has a solution for some real γ and $\eta = 0$ [26]. With help of $\eta \neq 0$ we can introduce exponential weights in order to tell the convective and absolute instabilities apart, as described in [25,26]. We can obtain the essential spectrum of the operator $\mathcal{M}$ solving the boundary problem (9) numerically with the continuation software AUTO. As a starting point, we can use a previously known eigenvalue and the corresponding eigenfunction, for instance, the Goldstone mode ($\lambda = 0, \gamma = 0, \mathbf{w}(\xi) = \partial_\xi \mathbf{u}_0(\xi)$), which is always present due to the translation symmetry of the problem.

We can also discretize both solution $\mathbf{u}_0(\xi)$ and operator $\mathcal{M}$ in order to solve the eigenvalue problem. We use the following two methods: (i) a finite-difference method on an adapted grid with approximation of the derivatives as described in [27] for separated and periodic boundaries and (ii) pseudo-spectral discretization in the Fourier-space for periodic boundary conditions. The last approach gives advantages with relatively smooth solutions, because the number of the treated modes can be significantly reduced without losing accuracy.

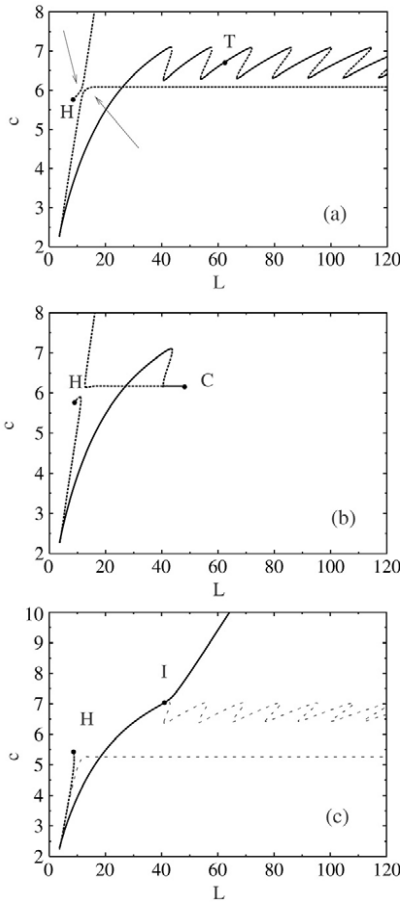

Fig. 4. (a) Dispersion relation for trigger and phase waves for $\phi = 8.42 \times 10^{-4}$. The dotted curve, originating from the H-point, represents limit cycles, unfolding from the Andronov–Hopf bifurcation. The curve with the comb-like upper branch is the dispersion relation of trigger waves. The arrows show the location of the up-coming transcritical collision between both curves. Here as in (b) and (c) solid (dashed) lines denote stable (unstable) solutions, respectively. (b) Both curves, just after the transcritical collision, $\phi = 8.41 \times 10^{-4}$. C denotes the turning point, see text. (c) Dispersion relation of phase waves at an even lower value $\phi = 8.0 \times 10^{-4}$. The thin dashed gray line shows the dispersion of trigger waves at a different ϕ value for sake of comparison. I denotes the inflection point, see text.

The finite-difference method on an adapted grid gives better results with strongly localized solutions. We use the Goldstone mode as an accuracy check in both discretization methods. We can also calculate points of the essential spectrum numerically with discretization and complete the underlying curve using the continuation technique.

2.4. Transition between phase and trigger waves: transcritical collision of dispersion curves

It turns out that this transition can be captured in the dispersion plane, where trigger and phase waves are clearly distinguishable by the shape of their dispersion curve. Postponing the thorough discussion of both wave types to the next sections, here we present the main result on the bifurcation scenario of the transition between phase and trigger waves.

Fig. 4(a) shows the initial situation before the transition: first, the line, which shows the limit cycles unfolding from the Andronov–Hopf bifurcation (see section "Phase waves") of the equilibrium in the travelling wave ODE and, second, the dispersion of the trigger waves (Fig. 4(a)). Adjusting to $\phi = 8.41 \times 10^{-4}$ (Fig. 4(b)), the dispersion curve of the phase waves collides with the lower branch of the dispersion curve of the trigger waves. Looking at the resulting joint curve we see that the dispersion line descending from the Andronov–Hopf bifurcation goes now along the skeleton of the dispersion relation toward large L, nearly repeating its shape. After that the curve turns at the C point back and again goes toward infinity along the linear part of the dispersion relation. At $\phi = 8.2 \times 10^{-4}$ (Fig. 4(c)) we observe a simple dispersion curve, originating from the Andronov–Hopf bifurcation, with a linear part, which goes to infinity without winding around the "skeleton" structure of the trigger wave dispersion curve.

Concerning the position of the turning point C, we make the following observations. If ϕ is slightly smaller than the critical value $\phi_{tr} = 8.418 \times 10^{-4}$, the point C is located at large values of L. While departing with ϕ further from ϕ_{tr}, the point C shifts to the left and disappears. At $\phi = 8.2 \times 10^{-4}$ the curve leaves the skeleton in the I point, as described by Fig. 4(c). Point C is closely related to the disappearance of the trigger waves, since it gives the section of the line of saddle-node bifurcations of trigger waves (in three-dimensional parameter space (c, L, ϕ)) with parameter plane (c, L). The section of the saddle-node bifurcation line with plane (ϕ, c) is given by point *SN* in Fig. 10(a).

The parameter value ϕ_{tr}, at which the transcritical collision between dispersion curves of phase and trigger waves takes place, is doubtless the boundary, which delimits the regimes of phase and trigger waves. Above ϕ_{tr} there coexist stable trigger waves and unstable small-amplitude phase waves. Below the boundary the only waves which exist are phase waves. The value ϕ_{tr} is bracketed by the Andronov–Hopf bifurcation ϕ_{hb} and the canard explosion ϕ_c of the limit cycle in the kinetics of the reaction–diffusion system, see Fig. 3.

3. Trigger waves

As mentioned above, trigger waves are slow diffusion-dependent propagating structures. They can appear either as solitary pulses or form spatially periodic trigger wave trains. The dispersion curve and the stability properties of the latter are strongly determined by the type of decay behind the corresponding solitary pulse [15,28,29]. Three qualitatively different types of solitary pulses and dispersion curves of the accompanying wave trains are found under decrease of parameter ϕ (increase of excitability) in the reaction–diffusion system (1).

3.1. Solitary pulses

The reaction–diffusion system (1) supports propagation of solitary excitation pulses in the parameter region $\phi > \phi_c$. We can obtain the dependence of the pulse velocity on ϕ performing continuation of the corresponding homoclinic solution of Eq. (7) in the (ϕ, c) parameter plane (Fig. 5(a)).

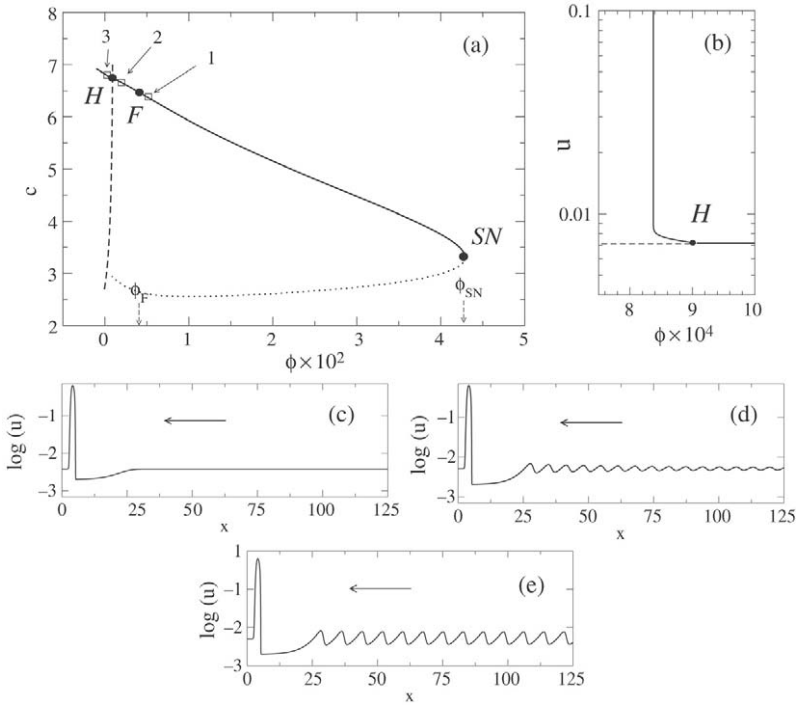

Fig. 5. (a) Dependence of the solitary pulse velocity on the ϕ parameter. *SN* denotes the saddle-node bifurcation (extinction threshold), *F* denotes the point of saddle to saddle-focus transition and *H* corresponds to the Andronov–Hopf bifurcation of the equilibrium. The solid line corresponds to stable solutions, the dotted — to unstable. The dashed line denotes the locus of the Andronov–Hopf bifurcation of the equilibrium in the travelling wave ODE. The extinction threshold is given by $\phi_{SN} = 4.29 \times 10^{-2}$, point *F* — by $\phi_F = 4.1 \times 10^{-3}$ and *H* point by $\phi_H = 9.0 \times 10^{-4}$. Labels 1, 2 and 3 mark the location of the pulses in panels (c)–(e). (b) Unfolding of the Andronov–Hopf bifurcation in the travelling wave ODE for a given value of c with a rapid canard-type growth of the amplitude of the new-born limit cycle. The Andronov–Hopf bifurcation for the given velocity c occurs at $\phi_H = 9.03 \times 10^{-4}$, and the canard explosion at $\phi_c = 8.38 \times 10^{-4}$. (c) Stable pulse profile for $\phi_F < \phi = 4.2 \times 10^{-3} < \phi_{SN}$. (d) Stable pulse profile for $\phi_H < \phi = 9.5 \times 10^{-4} < \phi_F$. (e) Pulse with undamped oscillatory tail for $\phi = 8.5 \times 10^{-4} < \phi_H$.

For a given ϕ value there simultaneously exist two pulses, one stable and one unstable. They collide in a saddle-node bifurcation *SN* at $\phi = \phi_{SN}$ parameter value (for comparison, see analytical results on the FitzHugh–Nagumo model in [30]). The present work focuses on the stable pulses belonging to the upper branch.

This branch is divided by point *F* (Fig. 5(a)). At this point the equilibrium in the travelling wave ODE (5) undergoes a saddle to saddle-focus transition and the homoclinic trajectory approaches the equilibrium in an oscillating manner. The equilibrium has for $\phi_H < \phi < \phi_F$ one unstable one-dimensional manifold (for the pulses, propagating to the left, as shown by Fig. 5), which describes the front of the pulse. The stable two-dimensional manifold with the corresponding complex-conjugated eigenvalues describes the decay behind the pulse (Fig. 5, compare panels (c) and (d)). For the pulses that move in the opposite direction with velocity $-c_0$, the fixpoint has contrariwise two unstable complex-conjugated eigenvalues that render the oscillatory tail of the pulse, and one stable eigenvalue, which is responsible for the front of the pulse.

With further decrease of the ϕ parameter the equilibrium of the profile equations undergoes an Andronov–Hopf bifurcation (point *H* in Fig. 5) at $\phi_H = 9.0 \times 10^{-4}$, and the pair of complex-conjugated eigenvalues crosses the imaginary axis, moving from the right to the left complex half-plane. The pulse solution below this bifurcation corresponds to a heteroclinic connection between the equilibrium and the small-amplitude limit cycle, born in the bifurcation point (Fig. 5(e)). This bifurcation is of very special meaning for the pulses in the reaction–diffusion system: it describes the appearance of undamped infinitely long tail oscillations behind the pulse. From the mathematical point of view, this is a cod-2 Shilnikov–Hopf bifurcation [31].

Now we turn to the stability properties of the solitary pulses. Pulses belonging to the faster branch, are found to be stable for $\phi_{hb} < \phi < \phi_{SN}$. We checked this fact by simulating the time evolution of the corresponding profiles. The essential part of the solitary pulse's spectrum is contained in the left half-plane, since the homogeneous background is stable for $\phi > \phi_{hb}$. The isolated eigenvalues were checked numerically by direct computation of the eigenvalues of the discretized linear operator.

Next, we discuss the pulses below the *H* point with the undamped oscillations in the tail. Numerical simulations reveal that they are stable on bounded domains due to the convective nature of the instability of the periodic wave train behind the pulse head (Fig. 6(b), see also section "Phase waves"). The essential spectrum of the small-amplitude wave train is shown on Fig. 6(a). The instability is of a long-wavelength type, since $\frac{d^2}{d\gamma^2}\mathrm{Re}(\lambda) > 0$ (see Eq. (9)) near the origin. Moreover, the instability is only convective, because we can shift the spectrum completely to the left half-plane, introducing an exponential weight $\eta \neq 0$ (see Eq. (9)). Simulations of the small-amplitude

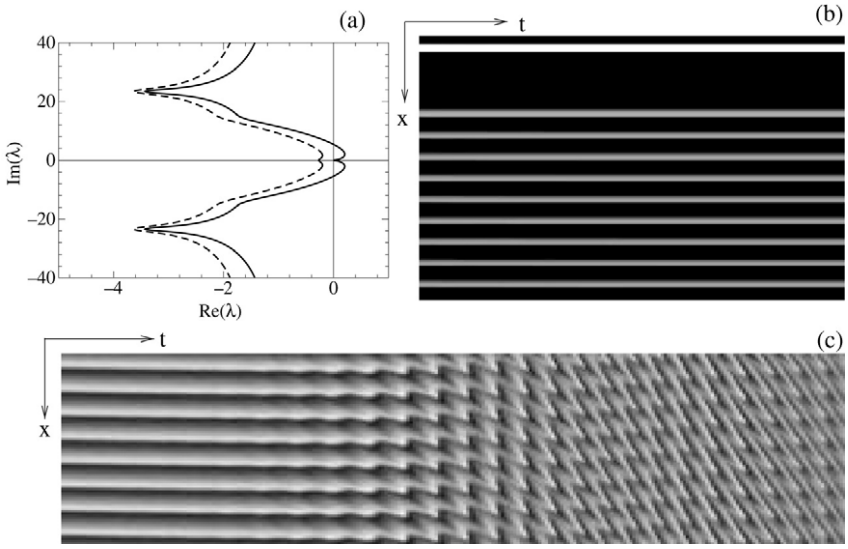

Fig. 6. (a) Solid line shows the leading part of the essential spectrum of the small-amplitude wave train behind the pulse head. Dashed line shows the spectrum in the weighted space with weight $\eta = 5.26 \times 10^{-1}$. (b) Space–time plot of a running solitary pulse in the co-moving frame. The logarithm of the u variable is coded in gray-scale with light (dark) colors corresponding to high (low) values, respectively. The simulations were made with Dirichlet boundary conditions in the front of the pulse and Neumann boundaries behind it. (c) Space–time plot of simulations of the periodic wave train, the color coding is renormalized to the actual maximal and minimal values of the variable. Periodic boundary conditions are applied.

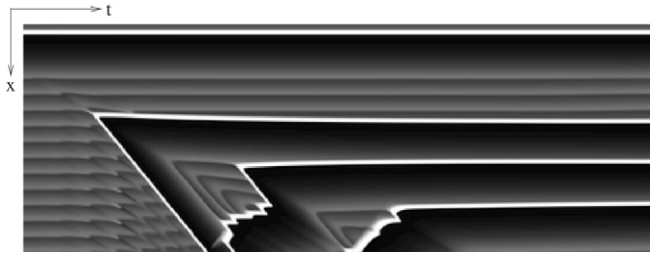

Fig. 7. Appearance of high-amplitude pulse heads behind the primary pulse ($\phi = 8.405 \times 10^{-4}$). Dirichlet boundary conditions, co-moving at the velocity of the solitary pulse coordinate system.

wave train with periodic boundaries uncovers the essential instability (Fig. 6(c)).

Under further decrease of parameter ϕ we see the phenomenon, which is often referred to as trace- and backfiring [20]. A pair of the high-amplitude pulse heads is born behind the primary pulse (Fig. 7). After a certain transient time, the whole domain behind the pulse is occupied by the high-amplitude wave train. A stationary pattern can be thought of as a heteroclinic connection between the equilibrium and a periodic orbit, representing the wave train, triggered by the running pulse. We would like to note that the discussed appearance of the new high-amplitude pulse heads seems also to be of the canard-like nature, because small changes in the parameter values lead to a significant transformation of the solution.

3.2. Trigger wave trains

Now we want to construct periodic wave trains of pulses with identical profiles. The interaction and stability of such wave trains will be determined mostly by the decay behind the corresponding solitary pulse, which was discussed in the previous subsection.

It was shown that the stability or instability of periodic wave trains is described by the so-called circle of critical eigenvalues, which was shown always to touch the origin [15]. This circle of eigenvalues appears as a blow-up of the isolated Goldstone eigenvalue of the primary solitary pulse. For $L \to \infty$ there is a correspondence between the slope of the dispersion and the location of the circle of critical eigenvalues. The wave trains belonging to the parts of the dispersion relation with negative slope are unstable with the circle of critical eigenvalues in the right half-plane. If L belongs to the part of the dispersion with positive slope, then the critical eigenvalues circle is in the left half-plane, reflecting the stability of the wave train.

In Fig. 8 we compare the type of the dispersion relation with the corresponding type of decay behind the associated solitary pulses (Fig. 5). Relatively low excitability of the system, which causes the tail of the solitary pulse to relax to the background state monotonously, results in a monotonous dispersion relation for the associated wave trains. After the transition from saddle to saddle-focus, marked as the F-point in Fig. 5(a), below which a solitary pulse displays damped tail oscillations, the dispersion curve becomes non-monotonous, combining parts with negative and positive slope.

The dispersion becomes non-monotonous, combining parts with negative and positive slopes. The periodic orbits contain a high-amplitude part and small-amplitude windings, whose number grows for large periods L. This picture is general for periodic orbits near a homoclinic connection of the Shilnikov type [31]. The interaction between the pulses in such a wave train, either attractive or repulsive, depends on the interpulse distance. Note also that there can coexist infinitely many wave trains with the *same velocity*, but of *different wavelengths*. Regarding the stability of the resulting wave trains, it was shown [15] that the wave trains change their stability periodically in L.

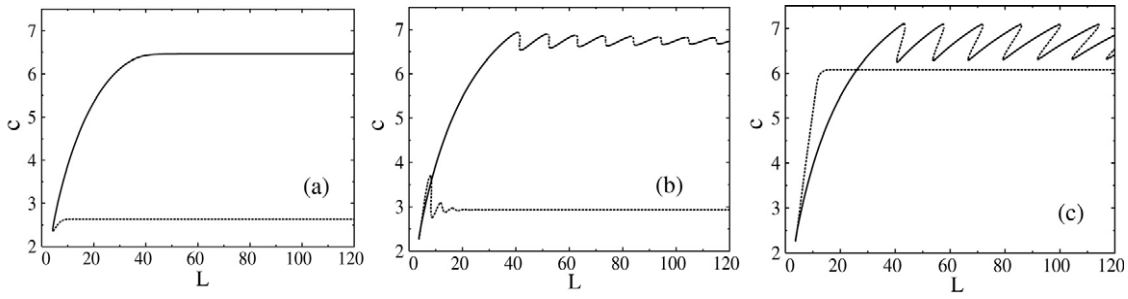

Fig. 8. Different dispersion curves of trigger wave trains as parameter ϕ is decreased (increasing excitability). Solid lines show stable solutions, dashed lines show unstable solutions. (a) Just above the F point, $\phi = 4.2 \times 10^{-3}$. Solitary pulse has monotonously decaying tail, compare with Fig. 5(c). (b) Between the Andronov–Hopf bifurcation and the F point, $\phi = 9.5 \times 10^{-4}$. Solitary pulse has decaying oscillatory tail, compare with Fig. 5(d). (c) Below the Andronov–Hopf bifurcation $\phi = 8.5 \times 10^{-4}$. Solitary pulse has non-damped oscillatory tail, compare with Fig. 5(e).

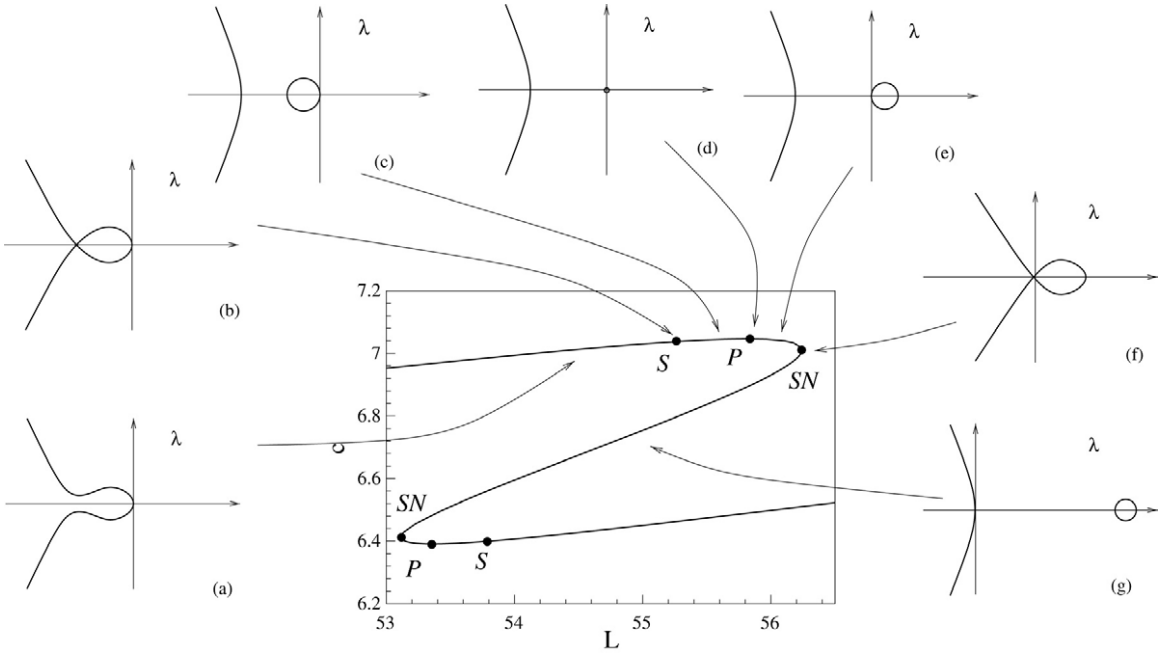

Fig. 9. In the center: a part of the bistable dispersion relation. The plots (a)–(f) illustrate the essential spectra of the wave trains for the different parts of the dispersion relation. (a) Stable wave trains. (b) Detaching of the critical eigenvalues circle from a spectral curve. (c) The circle of critical eigenvalues lies in the left half-plane. (d) The circle of critical eigenvalues shrinks to the origin. (e) The circle of critical eigenvalues flips to the right side of the λ plane. (f) Two spectral curves, touching the origin. (g) The circle of critical eigenvalues is detached from the origin.

Crossing the line of the Andronov–Hopf bifurcation under decrease of ϕ, we observe a qualitatively new type of dispersion curve (Fig. 8(c)). From the dynamical systems viewpoint, we have a codimension-zero situation with two homoclinic trajectories to the limit cycle, accompanied by a set of periodic orbits. These periodic orbits form a wiggly curve with saddle-node points, accumulating at homoclinic tangencies [31,32], which represent in our case two solitary pulses on a periodic background. The small-amplitude windings of the limit cycles are very close to the small periodic orbit, which was born in the Andronov–Hopf bifurcation. Another important feature of this dispersion is the presence of domains of bistability. Every such section contains three coexisting wave train solutions, two of them are stable and separated by an unstable one (see the central plot in Fig. 9). This phenomenon was first reported in [19].

Now let us take a closer look at the linear stability of the coexisting wave trains. For this purpose we calculate the essential spectra of the waves for different parts of the dispersion relation (Fig. 9). Far away from the extrema of the dispersion curve we find a single spectral curve, going through the origin of the complex λ plane (Fig. 9 (a)). Then, crossing point S (Fig. 9(b) and (c)), a separate closed spectral curve is nucleated from the rest of the spectrum. This curve is the circle of critical eigenvalues, which can be thought of as a blow-up of the Goldstone mode of the solitary pulse [15]. So the whole spectrum of the trigger wave breaks up into two pieces: the spectrum of the background small-amplitude wave and the circle, originating from the Goldstone mode of the primary solitary pulse.

In point P the wave train loses stability, and the circle of critical eigenvalues flips from the left to the right

halfplane (Fig. 9(c)–(e)). Up to the accuracy of the numerical computations, this flipping occurs as follows: the size of the circle first decreases, it blows off, becoming a dot in point P, and then the circle puffs out on the opposite side of the imaginary axis. In point P condition $\frac{dc}{dL} = 0$ holds. Thus, flipping of the circle of the critical eigenvalues coincides with the change of the slope of the dispersion curve $c(L)$. The interaction between the successive waves in a wave train, which belongs to the P–SN part of the dispersion relation is attractive, which provides the instability with respect to a shift of particular waves in the wave train.

Moving across the next extremum SN ($\frac{dL}{dc} = 0$), we find another qualitative change of the stability properties. First, in point SN there are two spectral curves that touch the origin (Fig. 9(f)). Under moving along the dispersion curve further (actually, in the opposite direction toward smaller L), the circle of critical eigenvalues detaches from the origin (Fig. 9(g)), but the second spectral curve remains attached to zero, as forced by the translation invariance of the problem.

Going along the dispersion curve further, we observe the reversed scenario: the detached circle of critical eigenvalues moves back to the origin, attaches to zero in the lower point SN (Fig. 8, the central plot), flips back to the left half-plane and unites with another spectral curve. We conclude, the wave trains are unstable between the S points in the dispersion relation. Up to the specific locations of the S, P and SN points this instability scheme is qualitatively the same for all overlapping regions of the wiggly dispersion curve.

The instability between points P and SN differs from that of the middle branch between two points SN. The first one (between P and SN) can be observed considering two equidistant pulses on a ring of length $2L$. There is an unstable eigenfunction of period $2L$. The instability between two points SN of the middle part of the bistable region is already seen with one pulse on a ring of length L, since there exists an unstable eigenfunction of period L.

We also would like to note that the sign of the slope of the dispersion coincides in our case with the curvature of the spectrum at the origin. For the parts of the dispersion with positive slope we find positive curvature of the spectrum, but there may exist another branch of the spectrum, the right complex half-plane (see the case with the detached circle of critical eigenvalues).

A thorough reader can raise the following question: how can a wave train with *unstable* small-amplitude wave pieces between the high-amplitude pulse heads be *stable*? We can argue with the following consideration. As was shown in [33], a wave can be stable, although separated pieces of its structure are *convectively* unstable, but *absolutely* stable (for the definitions of absolute and convective instabilities see [25]). In our case the small-amplitude waves behind the pulse heads are only *convectively* unstable. We did not compute the absolute spectrum of them, but the stabilization of the spectrum in a weighted space gives us a hint for the absolute stability of the small-amplitude waves.

The last part of this section on trigger waves we would like to address to their instabilities, caused by an increase of the excitability of the system (decrease of ϕ). Let us take a look at the dependence of the velocity of a particular trigger wave train of wavelengths $L = 48$ on parameter ϕ. We chose this wavelength, because the corresponding wave train belongs to the middle of the stable branch of the dispersion curve and is not subjected to the instability, which is related to the circle of critical eigenvalues and negative slope of the dispersion curve. In point U the wave train becomes unstable, this instability is of long-wavelength type, as can be seen from Fig. 10(b). Numerical simulations (Fig. 10(c)) reveal that the wave head tends to solder with the minor maximum in front of it, effectively increasing the propagation velocity of the whole wave train. After a long transient process (not shown in Fig. 10(c)), we obtain a new wave train without secondary maxima between the successive pulse heads, propagating at a larger velocity (see Section 4 below).

In point SN in Fig. 10(a) two limit cycles which belong to the upper respectively lower branch of the dispersion curve collide (see Fig. 8(a)). We conclude that under decrease of parameter ϕ the trigger waves first become unstable and subsequently disappear in a saddle-node collision with their twins belonging to the lower dispersion branch.

4. Phase waves

Phase waves are simpler objects than trigger wave trains in the sense that their form and properties do not depend on the wavelength as dramatically.

If $\mathbf{u}(\xi)$ is a periodic solution of (5), then, introducing a new variable $\zeta = c\xi$, we get:

$$\mathbf{f}(\mathbf{u}) + \partial_\zeta \mathbf{u} + c^{-2}\mathbf{D}\partial_\zeta^2 \mathbf{u} = 0.$$

In the limit of fast waves, $c \to \infty$, the diffusive term can be neglected ($c^{-2} \to 0$), and we end up with

$$\partial_\xi \mathbf{u} = -c^{-1}\mathbf{f}(\mathbf{u}). \tag{10}$$

We read from the (10) that the profile of the fast periodic solution $\mathbf{u}(\xi)$ is given by the corresponding periodic orbit in the kinetics of the system with reversed variable ξ. Moreover, we conclude that the propagation velocity acts as a period-scaling factor. If $\mathbf{u}(\xi)$ is a periodic solution, then c scales its period, providing the observed linear dispersion relation of phase waves at large c. Homogeneous bulk oscillations can be thought of as a degenerated example of phase waves propagating at infinite velocity.

Starting with initial values (ϕ_{hb}, ∞), which correspond to the appearance of homogeneous oscillations (Andronov–Hopf bifurcation in the kinetics), continuation of the locus of the Andronov–Hopf bifurcation in the (ϕ, c) parameter plane gives the curve depicted in Fig. 11(a). In order to get different dispersion curves of phase waves, we can just unfold the bifurcation in the (c, L) parameter plane for different values of ϕ (Fig. 11(b)).

There are two qualitatively different scenarios of the unfolding of the phase waves from the Hopf bifurcation. The result of the first one is the appearance of large-amplitude phase waves. This scenario occurs for smaller values of ϕ, see the

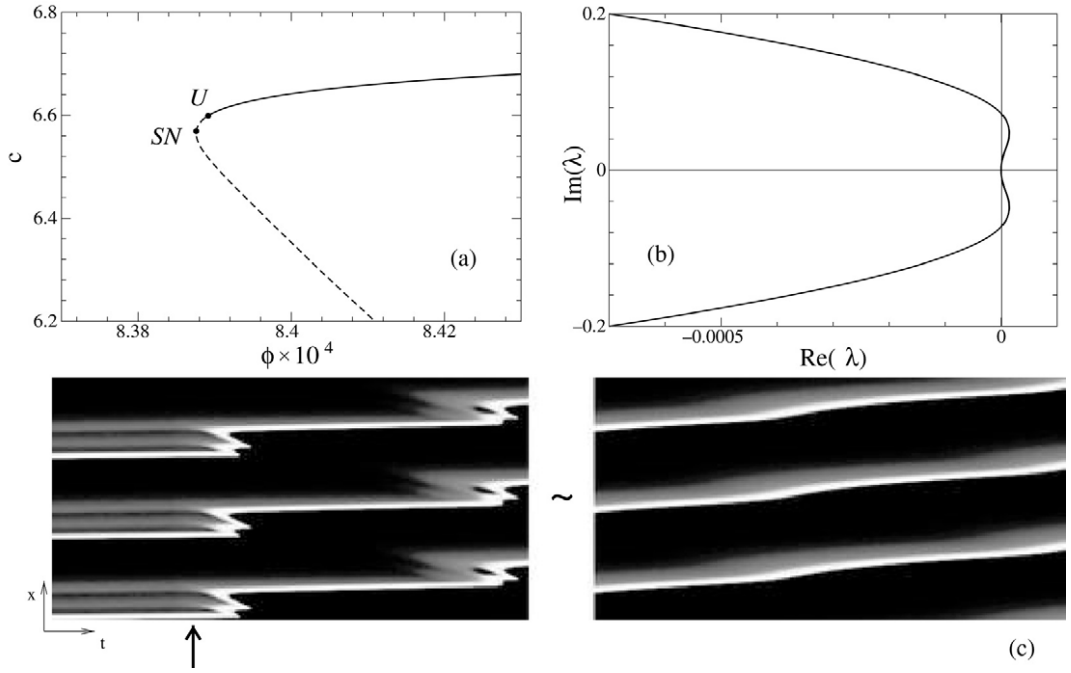

Fig. 10. (a) Bifurcation diagram for a particular trigger wave train, showing the instability point U and the point of the saddle-node collision with the twin wave train, belonging to the slower unstable dispersion branch. (b) Leading part of the eigenvalue spectrum of trigger wave train between U and SN points. (c) Space–time plot of a numerical simulation displaying the destruction of a trigger wave train. The parameter ϕ was initially set to $\phi = 8.4 \times 10^{-4}$ and than changed to the value $\phi = 8.0 \times 10^{-4}$. The arrow shows the parameter adjustment. The long transition process between the first and the last parts of the plot is cut out.

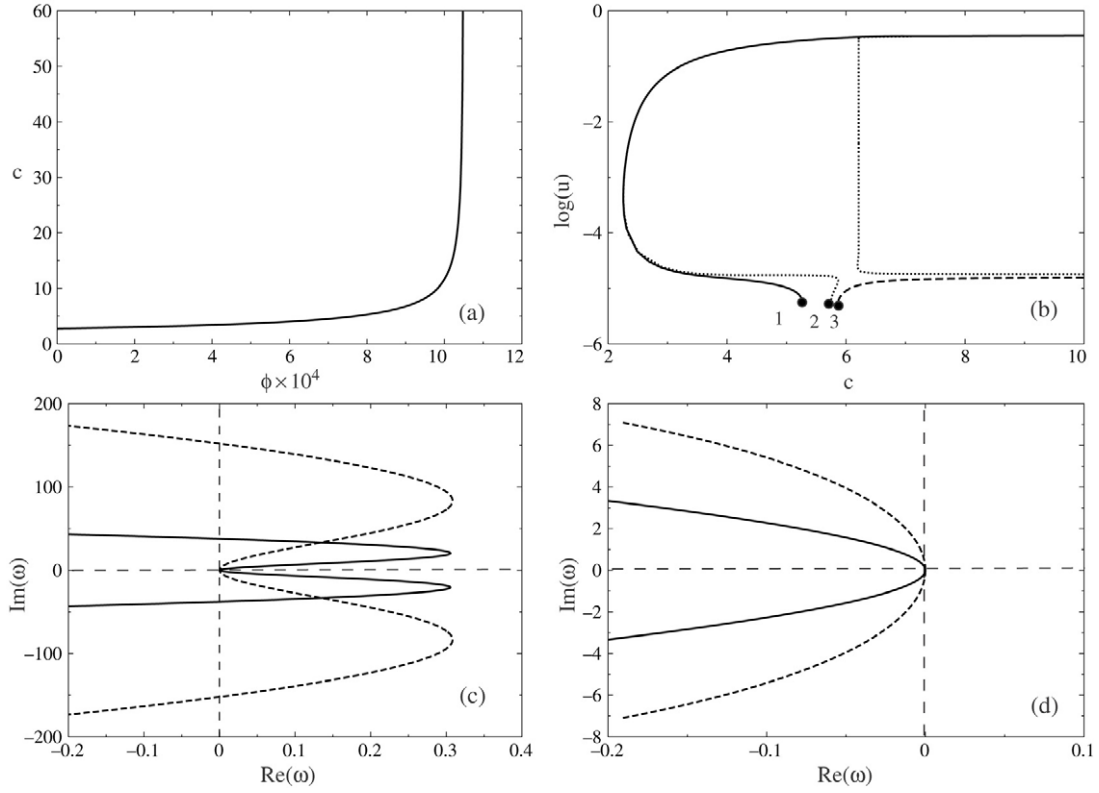

Fig. 11. (a) Locus of the Andronov–Hopf bifurcation in the (ϕ, c) parameter plane. (b) Three different scenarios of the unfolding of the limit cycles from the Hopf bifurcation. Solid line, originating from point 1: $\phi = 8.0 \times 10^{-4}$. Dotted line, originating from point 2: $\phi = 8.41 \times 10^{-4}$. Dashed line, originating from point 3: $\phi = 8.5 \times 10^{-4}$. (c) Spectra of the small amplitude phase waves at $\phi = 8.5 \times 10^{-4}$: solid (dashed) line corresponds to wavelength $L = 50$ ($L = 200$). (d) Spectra of the large amplitude phase waves at $\phi = 8.0 \times 10^{-4}$: solid (dashed) line corresponds to wavelength $L = 50$ ($L = 100$).

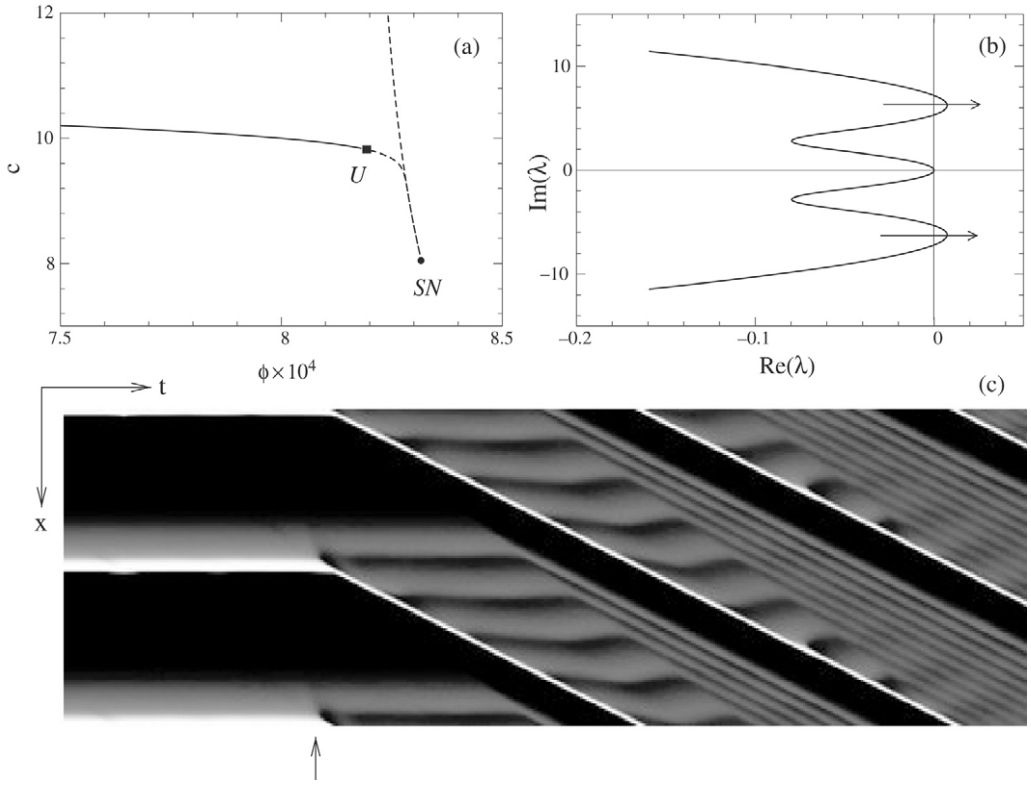

Fig. 12. (a) Dependence of the propagation velocity of a phase wave train on the ϕ parameter. The U point denotes the instability of the wave train, the corresponding ϕ value is $\phi_U = 8.22 \times 10^{-4}$. The *SN* points denotes a saddle-node bifurcation of the corresponding limit cycles in the travelling wave ODE. (b) Part of the essential spectrum of the unstable phase wave train slightly above the U point, $\phi = 8.23 \times 10^{-4}$ (c) Space–time plot of phase wave train in the co-moving frame, subjected to parameter jump from $\phi = 8.0 \times 10^{-4}$ to $\phi = 8.5 \times 10^{-4}$. Logarithmic grayscale coding and co-moving frame coordinates as in the figures above. The vertical arrow shows the moment of the parameter switching.

solid line in Fig. 11(b). After a large loop the velocity of the wave together with the wavelength go to infinity, while the profile remains the same. If we unfold the bifurcation at a large value of parameter ϕ, a large-amplitude wave doesn't emerge, see Fig. 11(b), the long-dashed line. The profile of the wave again converges against the limit cycle of the kinetics as the velocity and the wavelength go to infinity. There are also some intermediate scenarios, in which the wave first achieves the full amplitude, but then becomes smaller again (Fig. 11(b), short-dashed line).

We found that the small-amplitude phase waves are unstable in the whole wavelength range up to infinity (Fig. 11(c)). Changing the wavelength and the velocity of the wave just scales the spectrum of it in respect to the imaginary axis. The large-amplitude phase waves are found to be stable in the whole wavelength range with the same scaling properties of their spectrum (Fig. 11(d)).

Now we would like to describe the instabilities of the phase waves under variation of the excitability. We take a particular phase wave and increase the parameter ϕ. As we can see from the bifurcation diagram and the essential spectrum of the wave (Fig. 12(a) and (b)), the phase wave train becomes linearly unstable. This instability occurs at a finite wavelength. Numerical simulations (Fig. 12(b)) show that the instability of the phase waves leads to the transitory appearance of a secondary maximum between two successive high-amplitude wave parts. The wave tries to "localize" itself, tending to form a trigger wave train, which propagates at a slower velocity.

Let us compare the destruction of phase waves under ϕ increase and the break-up of trigger waves while the parameter ϕ is decreased. Both Figs. 10(c) and 12(c) look very similar under reversion of time. Whereas the high-amplitude heads of the trigger waves tends to merge with the next maximum, the high-amplitude part of the phase wave train breaks down, sprouting a new small-amplitude maximum in front of it.

5. Discussion and outlook

In this paper we reveal fine details of the transition between phase waves and triggers waves in a general two-component reaction–diffusion system with a cubic nonlinearity and well-separated time scales. The kinetics of the system can be controlled with a single parameter between excitable and oscillatory dynamics. Trigger waves and phase waves are "natural" spatial solutions for those two types of the kinetics.

The scheme of the transition between trigger and phase waves includes: (i) emergence of oscillations behind the solitary pulse, first damped. These cause damped oscillations in the dispersion relation of trigger wave trains. (ii) introduction of phase waves via the Andronov–Hopf bifurcation in the

travelling wave ODE, first at infinite velocity (bifurcation in the kinetics), then continuously in the comoving frames with the appropriate velocity. The oscillations in the decay behind the solitary pulse and in the dispersion of trigger wave trains become undamped. (iii) The transcritical collision of the phase wave dispersion with the dispersion of trigger waves. (iv) Successive disappearance of trigger waves of large periods in a series of saddle-node bifurcations. Similar results on the studied transition were obtained for FitzHugh–Nagumo and Barkley models [34], which suggests that the observed scenario is generic for the whole class of active media, possessing in dependence on a parameter both excitable (with one fixpoint) and oscillatory kinetics.

We present results of the linear stability analysis of phase and trigger waves belonging to the colliding dispersion curves. The spectra of trigger wave trains in the bistable domains are exhaustively analyzed. We find a good agreement between the slope of the nonlinear dispersion and the curvature of the spectrum in the origin, even for relatively low wavelengths L. We report also on the phenomenon of detached circle of critical eigenvalues for trigger wave trains belonging to the unstable part of the bistable domains. For phase waves, we find that small-amplitude phase waves are unstable in the whole range of wavelengths and the full-developed, high-amplitude phase waves are stable.

With the presented results of numerical simulations in hand, we strongly believe that the *experimental verification* of the reported scenario of the transition between phase and trigger waves should be the next research step on this field. One of the main objectives of the experimental proof is the existence of the small-amplitude phase waves, which play quite a deciding role in our study and which are experimentally not yet found to the best of our knowledge. However, the experimental evidences of trace- and backfiring can be thought of as hints for the existence of these small-amplitude oscillations.

From the mathematical viewpoint, our results could also stimulate the theory of the Shilnikov–Hopf bifurcation, since we don't find a good direct mathematical description of the observed phenomenon of collision of two different periodic solution branches in the "parameter-period" plane. Although the undamped dispersion curve are well known to mathematicians, the overlapping parts in a wiggly dispersion curve still need a theoretical clarification.

The last question is related to the connection between bifurcation of the objects in the travelling wave ODE and the stability of the corresponding solutions in the whole PDE. Sometimes we find a close correspondence between them (see the branches of the periodic solutions in "parameter-period" plane), but there are also observations, where the solution in the whole PDE becomes unstable in a regular point of the solution branch of the travelling wave ODE (see, for example, instability of trigger and phase waves under variation of parameter ϕ, Figs. 10(b) and 12(b)).

Acknowledgements

We thank B. Sandstede, A. Scheel and J. Rademacher for useful and motivating discussions during their stay at the TU Berlin. This study was supported by DFG in the frame of SFB 555.

References

[1] A.S. Mikhailov, Foundation of Synergetics 1, Distributed Active Systems, Springer, Berlin, 1991.
[2] R. Kapral, K. Showalter (Eds.), Chemical Waves and Patterns, Kluwer Academic Publishers, 1995.
[3] J. Ross, S.C. Müller, C. Vidal, Chemical waves, Science 240 (1988) 460–645.
[4] M. Cross, P.C. Hohenberg, Pattern formation outside of equilibrium, Rev. Modern Phys. 65 (1993) 851–1112.
[5] J. Tyson, J. Keener, Singular perturbation theory of travelling waves in excitable media (a review), Physica D 32 (1988) 327.
[6] Y. Kuramoto, Chemical Oscillations, Waves, and Turbulence, Springer-Verlag, Berlin, 1984.
[7] W. Eckhaus, Studies in Non-linear Stability Theory, Springer-Verlag, Berlin, 1965.
[8] A.C. Newell, J.A. Whitehead, Finite bandwidth, finite amplitude convection, J. Fluid. Mech. 38 (1969) 279.
[9] P. Ortoleva, J. Ross, Phase waves in oscillatory chemical reaction, J. Chem. Phys. 58 (1973) 5673–5680.
[10] E.J. Reusser, R.J. Field, The transition from phase waves to trigger waves in a model of the Zhabotinskii reaction, J. Amer. Chem. Soc. 101 (5) (1979) 1063–1071.
[11] R.R. Aliev, V.N. Biktashev, Dynamics of the oscillation phase distribution in the BZ reaction, J. Phys. Chem. 98 (1994) 9676–9681.
[12] C. Elphick, E. Meron, J. Rinzel, E.A. Spiegel, Impulse patterning and relaxational propagation of excitable media, J. Theor. Biol. 146 (1990) 249–268.
[13] C. Elphick, E. Meron, E.A. Spiegel, Spatiotemporal complexity in travelling patterns, Phys. Rev. Lett. 61 (5) (1988) 496–499.
[14] A.T. Winfree, Alternative stable rotors in an excitable medium, Physica D 49 (1991) 125–140.
[15] B. Sandstede, A. Scheel, On the stability of periodic travelling waves with large spatial period, J. Differential Equations 172 (2001) 134–188.
[16] H.U. Bödeker, A.W. Liehr, T.D. Frank, R. Friedrich, H.-G. Purwins, Measuring the interaction law of dissipative solitons, New J. Phys. 6 (2004) 62.
[17] C.P. Schenk, P. Schütz, M. Bode, H.-G. Purwins, Interaction of self-organized quasiparticles in a two-dimensional reaction-diffusion system: The formation of molecules, Phys. Rev. E 57 (1998) 6480–6486.
[18] M. Bode, A.W. Liehr, C.P. Schenk, H.-G. Purwins, Interaction of dissipative solitons: Particle-like behaviour of localized structures in a three-component reaction-diffusion system, Physica D 161 (2002) 45–66.
[19] G. Bordiougov, H. Engel, Oscillatory dispersion and coexisting stable pulse trains in an excitable medium, Phys. Rev. Lett. 90 (14) (2003) 148302.
[20] J. Rademacher, Ph.D. Thesis, University of Minnesota, 2004.
[21] H.-J. Krug, L. Pohlmann, L. Kuhnert, Analysis of the modified complete Oregonator accounting for oxygen sensitivity and photosensitivity of Belousov–Zhabotinsky reaction, J. Phys. Chem. 94 (1990) 4862–4865.
[22] M. Brøns, K. Bar-Eli, Canard explosion and excitation in a model of Belousov–Zhabotinsky reaction, J. Phys. Chem. 95 (1991) 8706–8713.
[23] E. Doedel, R. Paffenroth, A. Champneys, T. Fairgrieve, Y. Kuznetsov, B. Oldeman, B. Sandstede, X. Wang, AUTO2000: Continuation and bifurcation software for ordinary differential equations (with HOMCONT), Concordia University, Montreal, 2002.
[24] B. Sandstede, Stability of travelling waves, in: B. Fiedler (Ed.), Handbook of Dynamical Systems, North-Holland, 2002.
[25] B. Sandstede, A. Scheel, Absolute and convective instabilities of waves on unbounded and large bounded domains, Physica D 145 (2000) 233.
[26] B. Sandstede, A. Scheel, Absolute versus convective instability of spiral waves, Phys. Rev. E 62 (6) (2000) 7708.
[27] B. Fornberg, A Practical Guide to Pseudospectral Methods, Cambridge University Press, 1998.
[28] R. Gardner, On the structure of the spectra of periodic travelling waves, J. Math. Pures Appl. 72 (1993) 415–439.

[29] R. Gardner, Spectral analysis of long wavelength periodic waves and applications, J. Reine Angew. Math 491 (1997) 149–181.
[30] M. Krupa, B. Sandstede, P. Szmolyan, Fast and slow waves in the FitzHugh–Nagumo equation, J. Differential Equations 133 (1997) 49–97.
[31] P. Hirschberg, E. Knobloch, Šil'nikov–Hopf bifurcation, Physica D 62 (1993) 202–216.
[32] A.R. Champneys, A.J. Rodriguez-Luis, The non-transverse Shil'nikov–Hopf bifurcation: uncoupling of homoclinic orbits and homoclinic tangencies, Physica D 128 (1999) 130–158.
[33] B. Sandstede, A.Scheel, Gluing unstable fronts and backs together can produce stable pulses, Nonlinearity 13 (2000) 1465–1482.
[34] G. Röder, Diploma Thesis, Technische Universität Berlin, 2005.